

Interference and Coulomb interaction effects in counting statistics of electron transport through quantum dots

Sven Welack,* Massimiliano Esposito,† Upendra Harbola, and Shaul Mukamel‡
Department of Chemistry, University of California, Irvine, California 92697, USA.

Signatures of coulomb coupling and quantum interference in electron counting statistics through a pair of parallel quantum dots in a junction are investigated in a simulation study based on the generating function technique for a quantum master equation. Comparison is made with a single dot where interference is absent. The first three cumulants of the charge transfer distribution are predicted. The skewness and the average residence time of electrons in the dots are shown to be most sensitive to interferences and Coulomb coupling. Two point probability functions for elementary electron transfer processes show temporal oscillations due to interference. We verify that the steady-state fluctuation theorem which provides a universal connection between the number of forward and backward transfer events holds in the presence of electron-electron coupling and interference.

I. INTRODUCTION

Fast and sensitive charge detectors and highly stable current bias sources have made it possible to measure individual crossings of electrons through arrays of tunnel junctions¹ and quantum dots²⁻⁴ (QDs). Directional forward and reverse counting through two quantum dots in series has been reported⁵. A point contact is coupled asymmetrically to the dots to measure a trajectory of transitions between the charge states of the two dots. Spurred by this experimental progress, electron counting statistics in nanosystems has attracted recent theoretical interest⁶⁻¹⁷. Counting statistics of single electron transport was calculated for quantum dots coupled in series¹⁴ and parallel¹⁷ including decoherence. Counting statistics was also studied in the Coulomb blockade^{18,19}. It was shown that strong Coulomb interaction can suppress large current fluctuations¹⁸. Including quantum interference effects on current fluctuations revealed super-Poisson shot noise and the statistical signature of fast and slow transport channels¹⁹. Also, individual probabilities for spin-up and spin-down electron tunneling were calculated in the limit of strong Hubbard coupling.¹⁵ The quantum master equation approach (QME) is commonly used to study the electron counting statistics (ECS) through a system coupled to leads. When the rotating wave approximation (RWA) is applied to the QME^{6,20}, the coherences in the system eigenbasis become decoupled from the populations which obey a Pauli rate equation. Using the terminology of¹⁹, we denote the coupling between populations and coherences as interferences. The effects of interferences on the average currents crossing two coupled quantum dots have been studied

in Ref.²⁰ and on the ECS in a two-channel system in Coulomb blockade in Ref.¹⁹.

In this paper we extend this study to arbitrary Coulomb coupling in a model of two parallel QDs each containing a single spin orbital. We find that the third moment and the average electron residence time in the system provide useful indicators for interferences effects on the ECS. Counting statistics in systems with interferences can be realized experimentally by connecting two parallel QDs to two electrodes. The state transitions can be measured by employing a quantum point contact. As a reference point for the two parallel QDs, we calculate the corresponding values for a QD with a single orbital where interferences are absent. Electron counting statistics experiments have been proposed recently⁶ as good candidates to test the validity in the quantum domain of far-from-equilibrium fluctuation relations, called fluctuation theorems (FTs), which have recently raised a lot of attention in classical systems²¹⁻²⁵. In Ref.⁶ noninteracting electron were considered and the RWA has been used on the QME. We demonstrate in this paper that the FT still holds when interferences and Coulomb repulsion effects are present. The paper is organized as follows: We present two Models, two parallel single spin orbital quantum dots and a single orbital quantum dot in sections (IB) and (IA), respectively. Equations of motion (EOM) for both models are derived in section (II). We then introduce the GF in section (III). In section (V) we derive elementary probabilities for different electron detector configurations. The numerical results are presented in (VI) and we summarize and conclude in section (VII).

A. Model A: Two parallel quantum dots

Model A consists of two quantum dots each containing a single spin orbital which are connected to two electron reservoirs as shown in Fig. 1. The Hamiltonian

$$H = H_S + H_R + H_{SR}, \quad (1)$$

*Electronic address: swelack@uci.edu

†also at: Center for Nonlinear Phenomena and Complex Systems, Universite Libre de Bruxelles, Code Postal 231, Campus Plaine, B-1050 Brussels, Belgium.

‡Electronic address: smukamel@uci.edu

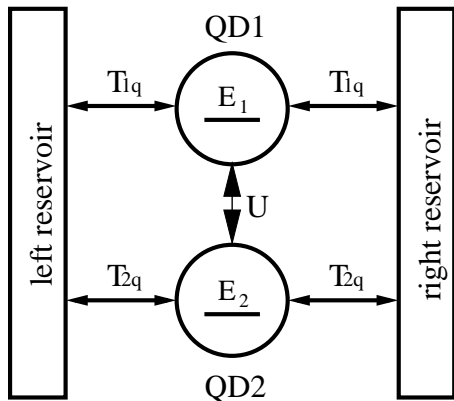


FIG. 1: Model A: Two model quantum dots, each has a single spin orbital with energy E_s , connected to a left and right electron reservoir. The left and right coupling elements are equal and also $T_{1q} = T_{2q}$, only the Fermi energies of the left and right lead are different, thus defining a bias voltage $V = E_{F,l} - E_{F,r}$. The Coulomb interaction between the two dots is parametrized by U .

consists of the system part H_S , the electron reservoir H_R , and their coupling term H_{SR} . We label the two dots with index $s = 1, 2$. In second quantization, the local-basis tight-binding Hamiltonian of the system part reads

$$H_S = \sum_{s=1}^2 E_s \Psi_s^\dagger \Psi_s + U \Psi_1^\dagger \Psi_1 \Psi_2^\dagger \Psi_2. \quad (2)$$

U is the Hubbard coupling strength. The environment consists of two independent electron reservoirs in thermal equilibrium. For each lead, the Hamiltonian H_R is given by

$$H_R = \sum_q \omega_q \Psi_q^\dagger \Psi_q \quad (3)$$

with Ψ_q^\dagger and Ψ_q create and annihilate an electron in the corresponding reservoir mode $|q\rangle$ with mode energy ω_q . To keep the notation simple, we will only refer to the left lead in further derivations. The right reservoir will be added to the final expressions. Since the leads are in thermal equilibrium, their occupation numbers are determined by Fermi-Dirac statistics

$$\langle \Psi_q^\dagger \Psi_{q'} \rangle_R = n_F(\omega_q - E_F) \delta_{qq'} \quad (4)$$

where $n_F(\omega) = 1/(e^{\beta\omega} + 1)$ is the Fermi function, $\beta = 1/kT$, and E_F the Fermi energy. We denote the trace over the reservoir degrees of freedom by $\langle \cdot \rangle_R = \text{tr}_R\{\cdot\}$. The coupling of the electronic lead with the system can be written as

$$H_{SR} = \sum_{sq} (T_{sq} \Psi_s^\dagger \Psi_q + T_{sq}^* \Psi_q^\dagger \Psi_s) \quad (5)$$

T_{sq} is the coupling strength between reservoir mode q and s -th QD.

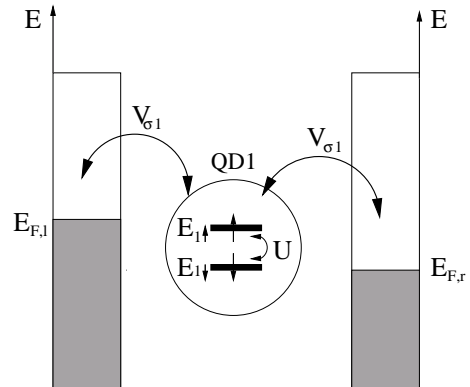


FIG. 2: Model B: A single orbital QD with energies $E_{1\uparrow}$, $E_{2\downarrow}$ for the spin-up and spin-down state. The coupled electronic reservoirs are in thermal equilibrium with Fermi energies $E_{F,l}$ and $E_{F,r}$. U is the electron-electron coupling parameter. The left and right coupling elements are equal and $V_{q\uparrow} = V_{q\downarrow}$

B. Model B: Single quantum dot

The second model consists of a single quantum dot with a single orbital which can accommodate two electrons with opposite spins coupled to two leads. In analogy to Model A, the total Hamiltonian can be written as $H = H_S + H_R + H_{SR}$. The system part is given by

$$H_S = \sum_{\sigma} E_{1\sigma} \Psi_{1\sigma}^\dagger \Psi_{1\sigma} + U \Psi_{1\uparrow}^\dagger \Psi_{1\uparrow} \Psi_{1\downarrow}^\dagger \Psi_{1\downarrow}. \quad (6)$$

Here, the spin is denoted by $\sigma = \uparrow, \downarrow$. The right reservoir was neglected in (6) but will be added in the final expressions. The Hamiltonian of the reservoir of electrons with spin reads

$$H_R = \sum_{q\sigma} \omega_q \Psi_{q\sigma}^\dagger \Psi_{q\sigma}. \quad (7)$$

Electrons with different spins in reservoir mode $|q\rangle$ have the same mode energy ω_q . The coupling term is given by

$$H_{SR} = \sum_q (V_{q\sigma} \Psi_{1\sigma}^\dagger \Psi_q + V_{q\sigma}^* \Psi_q^\dagger \Psi_{1\sigma}). \quad (8)$$

$V_{q\sigma}$ is the coupling strength between reservoir mode q and spin orbital σ . Even though both Model A and B can accommodate two electrons, there is a qualitative difference between the two. In Model B the operators of the reservoir have spin indices so that

$$\langle \Psi_{q\sigma}^\dagger \Psi_{q'\sigma'} \rangle = n_F(\omega_q - E_F) \delta_{qq'} \delta_{\sigma\sigma'}. \quad (9)$$

The additional $\delta_{\sigma\sigma'}$ in Eq.(9) compared to Eq.(4) will be important as shown later on.

II. EQUATIONS OF MOTION FOR THE REDUCED SYSTEM DENSITY MATRIX

Master equations have been widely used to simulate electron transport through quantum wires²⁶⁻³¹. Us-

ing a numerical decomposition of the reservoir spectral density^{32,33}, a non-Markovian master equation for electron transport was derived for non-interacting^{34,35} and interacting³⁶ electrons to second-order in H_{SR} . Higher order coupling elements can be derived via path-integral calculus²⁷. The approach is valid for arbitrary electron-electron coupling strength, temperature and bias. Master equations can be used to calculate the generating function (GF) that provides the charge transfer statistics of the system^{6,18,19}. Bi-directional counting requires relatively small bias voltages in order to have significant backwards transfer rates. Rather than substituting the Fermi function with a step function, we expand it in Matsubara-frequencies and can include small bias voltages into our calculations. We will use the density operator $\rho = |$ to describe the two models. We separate it into a system part ρ_S and a reservoir part ρ_R . From this point, we will refer to the system part ρ_S simply as density matrix and use a many-body four dimensional Fock space. Fock space coherences are present in the density matrix. We assume weak wire-lead coupling and no direct overlap (tunneling) between the wave functions of the left and right lead. For the quantum master equation in second-order perturbation theory in H_{SR} we get

$$\begin{aligned} \dot{\rho}_S(t) = & -i[H_S, \rho_S(t)] \\ & - \langle \mathcal{L}_{SR}(t) \int_{t_0}^t G(t, t') L_{SR}(t') G^\dagger(t, t') \rangle \rho_S(t) \end{aligned} \quad (10)$$

The Liouville operator is defined via $L_{SR} \cdot = [H_{SR}, \cdot]$ and the propagator is $G(t, t') = \exp(-iH_S(t - t'))$. We also set $\hbar = 1$. In order to propagate Eq. (10), we derive EOM for its dissipative part. These are presented in the following two subsections for Model A and B.

A. Quantum master equation for Model A

Applying the system-reservoir coupling term (5) of Model A to Eq. (10) we get³⁴

$$\begin{aligned} \dot{\rho}_S(t) = & -i[H_S, \rho_S(t)] \\ & \left\{ - \sum_s (\Psi_s^\dagger \Psi_s^{(+)}(t) \rho_S(t) + \Psi_s^\dagger \rho_S(t) \Psi_s^{(-)}(t)) \right. \\ & + \sum_s (\Psi_s^{(+)}(t) \rho_S(t) \Psi_s^\dagger - \rho_S(t) \Psi_s^{(-)}(t) \Psi_s^\dagger) \\ & \left. + h.c. \right\} \end{aligned} \quad (11)$$

We neglect the right lead for now. The auxiliary operators in Eq. (11) are given by

$$\Psi_s^{(+)}(t) = \sum_{s'} \int_{t_0}^t dt' C_{ss'}^{(+)}(t - t') G(t, t') \Psi_{s'}, \quad (12)$$

$$\Psi_s^{(-)}(t) = \sum_{s'} \int_{t_0}^t dt' \left(C_{ss'}^{(-)}(t - t') \right)^* G(t, t') \Psi_{s'}. \quad (13)$$

Because we assume that the coupling of the lead to the two dots is symmetric $T_{q1} = T_{q2}$, the reservoir correlation functions, given in Eqs. (A3, A4), which correspond the cross coupling terms, $s \neq s'$, can be written as $C_{ss'}^{(\pm)}(t - t') = C_{ss}^{(\pm)}(t - t')$. Setting $C_{ss'}(t) = 0$ for $s \neq s'$ would correspond to a rotating wave approximation²⁶. The correlation functions are discussed in more detail in Appendix (A). Liouville space provides a compact super operator notation. We define the following Liouville space super operators $\mathcal{L}A = [H_S, A]$, $\Psi^{(R)}A = A\Psi$, $\Psi^{(L)}A = \Psi A$, $\Psi^{\dagger(R)}A = A\Psi^\dagger$ and $\Psi^{\dagger(L)}A = \Psi^\dagger A$. A is an arbitrary operator in the space of the reduced system. We use R, L to denote left and right super operators and l, r as indices for the left and right lead. Eq. (11) finally reads

$$\dot{\rho}_S(t) = W_A(t) \rho_S(t) \quad (14)$$

where $W_A(t)$ is

$$W_A(t) \equiv -i\mathcal{L} - \Pi^l(t) + \Sigma_+^l(t) + \Sigma_-^l(t). \quad (15)$$

In Fock space, the dissipation terms are separated into a diagonal contribution

$$\Pi^l(t) = \sum_s \Psi_s^{\dagger(L)} \Psi_s^{(+,L)}(t) + \Psi_s^{\dagger(R)} \Psi_s^{(-,R)}(t) + h.c. \quad (16)$$

which leave the number of electrons in the system unchanged and off-diagonal parts

$$\Sigma_+^l(t) = \sum_s \Psi_s^{\dagger(L)} \Psi_s^{(-,R)}(t) + \Psi_s^{(R)} \Psi_s^{\dagger(-,L)}(t), \quad (17)$$

$$\Sigma_-^l(t) = \sum_s \Psi_s^{\dagger(R)} \Psi_s^{(+,L)}(t) + \Psi_s^{(L)} \Psi_s^{\dagger(+,R)}(t), \quad (18)$$

which increase or decrease the number of electrons, respectively. $W_A(t)$ is a 16×16 super operator. The terms for the right lead $\Pi^r(t)$, $\Sigma_+^r(t)$ and $\Sigma_-^r(t)$ can be derived by replacing $C_{ss'}^{(\pm)}$ in Eqs. (12,13) with the correlation functions of the right lead and have to be added to Eq. (15). In Appendix (A) we demonstrate a spectral decomposition of the reservoir correlation functions. It results in the representation $C_{ss'}^{(\pm)}(t) = \sum_{k=1}^{m+m'} a_k^{(\pm)} e^{\gamma_k^{(\pm)} t}$.

A numerically efficient way for calculating Eqs. (12,13) is by propagating the EOM

$$\begin{aligned} \frac{\partial}{\partial t} \Psi_{s,k}^{(\pm)}(t) = & \gamma_k^{(\pm)} \Psi_{s,k}^{(\pm)}(t) - i[H_S, \Psi_{s,k}^{(\pm)}(t)] \\ & + \sum_{s'} a_k^{(\pm)} \Psi_{s'}. \end{aligned} \quad (19)$$

Summing up over the spectral decomposition given by Eq. (A10) results in an explicit expressions for the many-body auxiliary $\Psi_s^{(\pm)}(t) = \sum_{k=1}^{m+m'} \Psi_{s,k}^{(\pm)}(t)$ operators. Eqs. (14 - 19) are propagated simultaneously in time and form a closed set for calculating the reduced density operator $\rho_S(t)$. An adiabatic switching of the coupling is

not required in this method. We are interested in electron counting statistics in steady state which we reach by propagating numerically $\rho_S^{st} = \rho_S(t \rightarrow \infty)$, $\Pi = \Pi(t \rightarrow \infty)$, $\Sigma_+ = \Sigma_+(t \rightarrow \infty)$ and $\Sigma_- = \Sigma_-(t \rightarrow \infty)$.

In this model the presence of interferences has been studied for non-interaction electrons on average currents²⁶ and on current statistics in the strong Coulomb blockade¹⁹. A rotating wave approximation (RWA) as applied in Ref.²⁶ cancels the interferences which couple the coherence part to the population part. We observe the same in our numerical investigation for arbitrary Coulomb coupling strength. Thus in the case of a RWA, Eq. (14) would reduce to a Pauli rate equation for Model A. In the following subsection, we show that the EOM for Model B is given by a Pauli rate equation without applying RWA explicitly. In Model B, the interference terms are zero due to the spin indices in the correlation functions (A1,A2).

B. Pauli rate equation for Model B

Inserting the system-reservoir coupling term (6) of Model B into Eq. (8), we can write

$$\begin{aligned} \dot{\rho}_S(t) = & -i[H_S, \rho_S(t)] \\ & \left\{ - \sum_{\sigma} (\Psi_{1\sigma}^{\dagger} \Psi_{1\sigma}^{(+)}(t) \rho_S(t) + \Psi_{1\sigma}^{\dagger} \rho_S(t) \Psi_{1\sigma}^{(-)}(t)) \right. \\ & + \sum_{\sigma} (\Psi_{1\sigma}^{(+)}(t) \rho_S(t) \Psi_{1\sigma}^{\dagger} - \rho_S(t) \Psi_{1\sigma}^{(-)}(t) \Psi_{1\sigma}^{\dagger}) \\ & \left. + h.c. \right\} \end{aligned} \quad (20)$$

The auxiliary operators in Eq. (20) are given by

$$\Psi_{1\sigma}^{(+)}(t) = \int_{t_0}^t dt' C_{\sigma\sigma}^{(+)}(t-t') G(t, t') \Psi_{1\sigma'}, \quad (21)$$

$$\Psi_{1\sigma}^{(-)}(t) = \int_{t_0}^t dt' \left(C_{\sigma\sigma}^{(-)}(t-t') \right)^* G(t, t') \Psi_{1\sigma'}. \quad (22)$$

The reservoir correlation functions $C_{\sigma\sigma}^{(\pm)}(t-t')$ are given in Eqs. (A1,A2). The master equation can be recast in the compact Liouville space form

$$\dot{\rho}_S(t) = W_B(t) \rho_S(t) \quad (23)$$

with

$$W_B(t) \equiv -i\mathcal{L} - \Pi^l(t) + \Sigma_+^l(t) + \Sigma_-^l(t). \quad (24)$$

The diagonal part is given by

$$\Pi^l(t) = \sum_{\sigma} \Psi_{1\sigma}^{\dagger(L)} \Psi_{1\sigma}^{(+,L)}(t) + \Psi_{1\sigma}^{\dagger(R)} \Psi_{1\sigma}^{(-,R)}(t) + h.c. \quad (25)$$

and off-diagonal parts by

$$\Sigma_+^l(t) = \sum_{\sigma} \Psi_{1\sigma}^{\dagger(L)} \Psi_{1\sigma}^{(-,R)}(t) + \Psi_{1\sigma}^{(R)} \Psi_{1\sigma}^{\dagger(-,L)}(t), \quad (26)$$

$$\Sigma_-^l(t) = \sum_{\sigma} \Psi_{1\sigma}^{\dagger(R)} \Psi_{1\sigma}^{(+,L)}(t) + \Psi_{1\sigma}^{(L)} \Psi_{1\sigma}^{\dagger(+,R)}(t). \quad (27)$$

Because $C_{\uparrow\downarrow}^{(\pm)} = C_{\downarrow\uparrow}^{(\pm)} = 0$ as shown in Appendix (A), the spin quantum number causes a separation of coherence and population part in the density operator²⁶. The population part of Eq. (23) satisfies the Pauli rate equation

$$\dot{P}_S(t) = W_P P_S(t). \quad (28)$$

P denotes the population of the states, W_P is the Pauli rate matrix.

III. THE GENERATING FUNCTION

The transfer probability of k electrons in the time interval $t - t_0$ through the left lead is $P(\mathbf{k}; t)$. We define the generating function $G(t, \boldsymbol{\lambda})$ by

$$P(\mathbf{k}; t) = \frac{1}{2\pi} \int_0^{\infty} d\lambda G(\boldsymbol{\lambda}; t) e^{-\boldsymbol{\lambda} \cdot \mathbf{k}}. \quad (29)$$

To calculate the Fourier transform (29), one can replace $\boldsymbol{\lambda}$ with $i\boldsymbol{\lambda}$ and change the integration limits to $P(\mathbf{k}; t) = \frac{1}{2\pi} \int_0^{2\pi} G(t, i\boldsymbol{\lambda}) e^{-i\boldsymbol{\lambda} \cdot \mathbf{k}}$. We will calculate the GF by tracing the generating operator^{6,19} (GO) $g(t, \boldsymbol{\lambda})$ over the system degrees of freedom

$$G(\boldsymbol{\lambda}; t) = \langle \langle I | g(t, \boldsymbol{\lambda}) \rangle \rangle_S. \quad (30)$$

Based on the master equation (23), the EOM is

$$\dot{g}(\boldsymbol{\lambda}; t) = W(\boldsymbol{\lambda}) g(\boldsymbol{\lambda}; t). \quad (31)$$

We start counting after the system has reached steady state. Thus the initial condition of the GO is given by the steady state of the system density matrix $g(\boldsymbol{\lambda}; t = 0) = \rho_S^{st}$. The propagator $W(\boldsymbol{\lambda})$ of the GO is

$$W(\boldsymbol{\lambda}) = -i\mathcal{L} - \Pi^l - \Pi^r + e^{\lambda_1} \Sigma_+^l + e^{\lambda_2} \Sigma_-^l + \Sigma_+^r + \Sigma_-^r. \quad (32)$$

We shall consider the statistics of charge transfers only between the left lead and the system. $\boldsymbol{\lambda} := (\lambda_1, \lambda_2)$ controls the specific statistics obtained by propagating Eq. (31). We investigate 3 cases. Setting $\boldsymbol{\lambda}_+ := (\lambda_1 = \lambda, \lambda_2 = 0)$ results in the counting statistics of the incoming electrons, $\boldsymbol{\lambda}_- := (\lambda_1 = 0, \lambda_2 = \lambda)$ the outgoing, and $\boldsymbol{\lambda}_n := (\lambda_1 = \lambda, \lambda_2 = -\lambda)$ the net-process. The corresponding probabilities are denoted $P^+(\mathbf{k}; t)$, $P^-(\mathbf{k}; t)$ and $P^n(\mathbf{k}; t)$, respectively.

IV. CUMULANTS OF THE TRANSFER DISTRIBUTIONS

We shall calculate the first $C_1(t)$, second $C_2(t)$ and third $C_3(t)$ cumulant of $P(\mathbf{k}; t)$ with respect to \mathbf{k} . $C_1(t) = \bar{k}/t = \sum_{\mathbf{k}} k P(\mathbf{k}; t)/t$ is related to the average current $I(t) = eC_1(t)$. The second cumulant is defined

by $C_2(t) = (\overline{k^2} - \bar{k}^2)/t$. It is commonly represented by the Fano factor $F(t) = \frac{C_2(t)}{C_1(t)}$. The third cumulant $C_3(t) = \overline{(k - \bar{k})^3}/t$ measures the skewness of the probability distribution $P(\mathbf{k}; t)$ with respect to k . For small bias, the current is small and the electrons transferring into the wire are uncorrelated. This leads to a Poisson counting statistics and the Fano factor equals $F = 1$. If $F < 1$, the process is Sub-Poissonian, while $F > 1$ indicates Super-Poissonian statistics.

The time-dependent cumulants can be calculated from

$$C_k^{(\eta)}(t) = (\partial_\lambda)^k K(t, \boldsymbol{\lambda}_\eta) \Big|_{\lambda=0} \quad (33)$$

where $K(t, \boldsymbol{\lambda})$ is obtained from the GF

$$K(t, \boldsymbol{\lambda}_\eta) = -\frac{1}{t} \ln(G(t, \boldsymbol{\lambda}_\eta)). \quad (34)$$

We make use of the fact, that $K(t, \boldsymbol{\lambda})$ has a well defined limit and calculate the asymptotic values⁶ for the steady state current

$$C_1^{(\eta)} = \frac{\partial}{\partial \lambda} \lim_{t \rightarrow \infty} K(t, \boldsymbol{\lambda}_\eta) \Big|_{\lambda=0} \quad (35)$$

and the zero frequency power spectrum

$$C_2^{(\eta)} = \frac{\partial^2}{\partial \lambda^2} \lim_{t \rightarrow \infty} K(t, \boldsymbol{\lambda}_\eta) \Big|_{\lambda=0}. \quad (36)$$

The asymptotic value of the skewness is defined in the same fashion

$$C_3^{(\eta)} = \frac{\partial^3}{\partial \lambda^3} \lim_{t \rightarrow \infty} K(t, \boldsymbol{\lambda}_\eta) \Big|_{\lambda=0}. \quad (37)$$

The long time limit of $K(t, \boldsymbol{\lambda}_\eta)$ can be calculated from the eigenvalues²⁰ $\epsilon_{i, \boldsymbol{\lambda}_\eta}$ of the propagator $W(\boldsymbol{\lambda}_\eta)$ given by Eq. (32). Then, $K(\boldsymbol{\lambda}_\eta) = \lim_{t \rightarrow \infty} K(t, \boldsymbol{\lambda}_\eta) = \epsilon_{1, \boldsymbol{\lambda}_\eta}$ for the eigenvalue with $\epsilon_{1, \boldsymbol{\lambda}_\eta} \rightarrow 0$ when $\boldsymbol{\lambda}_\eta \rightarrow 0$.

V. PROBABILITIES OF ELEMENTARY EVENTS

We introduce elementary probabilities to study consecutive electron transfer events m_1, m_2 at times t_1, t_2 . m characterizes the side of the process (l, r) and if the electron is transferred in (+) or out (-) of the QD. The elementary probability is given by^{37,38}

$$P(t_2, t_1) = \langle \Sigma^{m_2} S_{t_2, t_1} \Sigma^{m_1} S_{t_1, t_0} \rangle. \quad (38)$$

Eq. (38) is the joint probability of detecting specified electron transfers at times t_1 and t_2 without transfers occurring in the time intervals t_1, t_0 and t_2, t_1 . We denote the trace over the system degrees of freedom by $\langle \cdot \rangle = \text{tr}_S \{ \cdot \rho_S(t_0) \}$. S_{t_i, t_j} is the propagator of the system in absence of transfer events at the leads within the time interval t_i, t_j :

$$S_{t_i, t_j} = \exp((-i\mathcal{L} - \Pi^l - \Pi^r)(t_i - t_j)). \quad (39)$$

We consider three cases. *i*) An electron is detected when it enters the junction through the left lead at time $t_1 = 0$ and leaves the junction through the right lead at time t . The electron transfer operators are Σ_1^l and Σ_2^r respectively and we denote this transfer pathway by $l \rightarrow r$. Then the joint elementary probability is given by

$$P_{l \rightarrow r}(t, t_0) = \langle \Sigma_-^r S_{t, t_0} \Sigma_+^l \rangle. \quad (40)$$

ii) The reverse process, $r \rightarrow l$, which we write as

$$P_{r \rightarrow l}(t, t_0) = \langle \Sigma_-^l S_{t, t_0} \Sigma_+^r \rangle. \quad (41)$$

iii) The transfer from the left lead into the system and back into the left lead denoted by $l \rightarrow l$ can be written as

$$P_{l \rightarrow l}(t, t_0) = \langle \Sigma_-^l S_{t, t_0} \Sigma_+^l \rangle. \quad (42)$$

In all three cases, we assume continuous measurement of electrons and that no other events take place between t_0 and t .

Quantities (40-42) can be measured as follows. One has to detect single directionally resolved electron transfers between the leads and the system and record a time-series of transfer events. The time series has to be sufficiently long. Then a histogram of the number of occurrences of a specific consecutive transfer event, such as $l \rightarrow r$, as function of increasing time intervals $t - t_0$ can be generated. The histogram has to be normalized by the total number of events $\Sigma^{m_1} \rightarrow \Sigma^{m_2}$ in the time series.

The overall probability $P_{m_1 \rightarrow m_2}^c$ to have the $\Sigma^{m_1} \rightarrow \Sigma^{m_2}$ event in an infinite time series of electron transfer events irrespective of the time-interval between m_2 and m_1 can be calculated by integrating the conditional elementary probability $P_{m_1 \rightarrow m_2(\tau)}^c = \langle \Sigma^{m_2} S_{\tau, t_0} \Sigma^{m_1} \rangle / \langle \Sigma^{m_1} \rangle$:

$$P_{m_1 \rightarrow m_2}^c = \int_0^\infty d\tau \langle \Sigma^{m_2} S_{\tau, t_0} \Sigma^{m_1} \rangle / \langle \Sigma^{m_1} \rangle. \quad (43)$$

Other interesting quantities can be calculated based on Eq. (40-42). For example, the expected residence time of electrons in the system subject to a specific transfer process $m_1 \rightarrow m_2$. It is given by

$$t_{res} = \frac{\int_0^\infty d\tau \tau \langle \Sigma^{m_2} S_{\tau, t_0} \Sigma^{m_1} \rangle}{\int_0^\infty d\tau \langle \Sigma^{m_2} S_{\tau, t_0} \Sigma^{m_1} \rangle}. \quad (44)$$

We propose another interesting setup, by counting electrons only at the left lead. We do not keep track of the electron transfer through the right lead. Thus the propagator (39) is modified to

$$\tilde{S}_{t_i, t_j} = \exp((-i\mathcal{L} - \Pi^l - \Pi^r + \Sigma_+^r + \Sigma_-^r)(t_i - t_j)). \quad (45)$$

We calculate the conditional probability of an electron entering the system at time t_0 through the left lead, and the next electron entering at time t from the left lead. This can be written as

$$P_{l, l}^c(t|t_0) = \langle \Sigma_+^l \tilde{S}_{t, t_0} \Sigma_+^l \rangle / \langle \Sigma_+^l \rangle. \quad (46)$$

We denote this transfer series by l, l . In the time interval $t-t_0$ electron transfers take place only in the right lead. This can also be measured experimentally with a two detector setup when on filters the right transfer events out of the time series. For uncorrelated electron transfer, the propability distribution (46) is Poissonian and can be written as³⁹

$$P_{l,l}^{poiss}(t|t_0) = e^{-C_1 t} \langle \Sigma_+^l \rangle. \quad (47)$$

VI. NUMERICAL SIMULATIONS

In order to carry out the numerical calculations, we write all system operators in the many-body basis. For Model A we use the transformation

$$\Psi_s^\dagger = \sum_{mm'} \alpha_{mm'}^{(s)} |m\rangle \langle m'|. \quad (48)$$

The many body basis is spanned by four states $|0\rangle = |00\rangle$, $|1\rangle = |01\rangle$, $|2\rangle = |10\rangle$ and $|3\rangle = |11\rangle$. The coefficients of the transformation $\alpha_{mm'}^{(\dagger,s)}$ between orbital basis and many-body basis can be derived from the Fermion anti-commutator relations. Here the non-zero coefficients for the creation operators are $\alpha_{20}^{(1)} = 1$, $\alpha_{31}^{(1)} = 1$, $\alpha_{10}^{(2)} = 1$ and $\alpha_{32}^{(2)} = -1$. Thus we get $\Psi_1^\dagger = |10\rangle \langle 00| + |11\rangle \langle 01|$ and $\Psi_2^\dagger = |01\rangle \langle 00| - |11\rangle \langle 10|$. The annihilation operators can be derived by replacing $\alpha_{mm'}^{(s)}$ with $\alpha_{m'm}^{(s)}$. For Model B, one has to replace $s = 1$ with $\sigma = \uparrow$ and $s = 2$ with $\sigma = \downarrow$. Since there is no hopping element in Hamiltonians (2, 6), this representation is the many-body eigenbasis of the reduced system. We can write (2) and (6) as

$$H_S = \sum_{m=0}^3 \epsilon_m |m\rangle \langle m|. \quad (49)$$

ϵ_m is the eigenenergy of state $|m\rangle$. The energy settings we used for Model A and B are shown in Fig. (3). All energies are scaled with respect to the equilibrium chemical potential of the leads $\mu = 1$. The fixed orbital energies for Model A are $\epsilon_1 = E_1 = 0.999$, $\epsilon_2 = E_2 = 1.001$ and for Model B $\epsilon_1 = E_{1\uparrow} = 0.999$ and $\epsilon_1 = E_{1\downarrow} = 1.001$. Thus, the double occupancy state has an energy of $\epsilon_3 = E_1 + E_2 + U = 2.0 + U$. The ground state is set to zero $\epsilon_0 = 0$. The bias voltage is applied symmetrically to the system using $E_{F,l} = E_F + V/2$, $E_{F,r} = E_F - V/2$. Since we want to study temperature fluctuations of electron transfer as a function of U , we set $T = 0.002$ to be in a temperature range of $\beta V \approx U$. In Eq. (A6), we restrict the spectrum to a single Lorentzian centered at $\Omega_1 = E_F$. We also chose relatively large bandwidth parameter $\Gamma_1 = 1$ (wide-band limit). We set $p_1 = 2 \cdot 10^{-4}$ in Eq. (A6) ($p_1 \sim \sum_q |V_q|^2 = \sum_q |T_q|^2$) as a reasonable small value considering the weak coupling one has to assume in order to guarantee physical results within second-order perturbation theory.

$$\begin{array}{ccc} \epsilon_3 = & \underline{E_1 + E_2 + U} & \\ \underline{E_F = 1} & \epsilon_2 = \underline{E_2 = 1.001} & \underline{E_F = 1} \\ & \epsilon_1 = \underline{E_1 = 0.999} & \\ & \underline{\epsilon_0 = 0} & \end{array}$$

FIG. 3: Level scheme in many-body eigenbasis for Model A. For Model B, E_1 and E_2 have to be replaced by $E_{1\uparrow}$ and $E_{1\downarrow}$.

We use a Runge-Kutta method to propagate the EOM for Model A (14) and Model B (23) to get the steady state values of the single transfer operators (Σ) and the density operator. Based on those, we then propagate the EOM of the generating operator (31) to obtain the statistics.

A. Bidirectional transfer probability

In Fig. 4 we depict the probability $P(\mathbf{k}_n; t)$ of the number k of net-electron transfers between the left lead and the system at steady state. The time is fixed to $t = 200$. The left panel depicts Model A, the right panel Model B. The distributions for different electron-electron coupling strengths $U = 0$, $U = 2 \cdot 10^{-3}$ and $U = 8 \cdot 10^{-3}$ are fitted with a Gaussian $P(k) = \frac{\sqrt{w}}{2\sqrt{2}} \exp(-\frac{2}{w}(k - x_c)^2)$. The parameters are given in the graph. A small bias of $V = 4 \cdot 10^{-4}$ ensures electron transfers in reverse direction of the bias. As discussed for non-interacting⁶ and strongly coupled¹⁸ electrons, the Gaussian provides a good approximation for $P(\mathbf{k}_n; t)$ except for the tails. This is mainly due to small non-equilibrium contrains. For high bias, the deviations will be more significant. The electron-electron coupling U shifts the maximum of the Gaussian to smaller transfer numbers, increasing the overall probability of reverse transfer events. Furthermore an additional spreading of the probability is biased towards negative numbers. Thus, a significantly larger reverse process can be observed due to electron-electron coupling. When Coulomb interaction is present, interference effects are more pronounced. This can be seen by comparing the results for Models A and B in Fig. 4.

B. Cumulants

The cumulants as derived from the GF in section (III) are of special interest since they are directly related to transport properties. In the following, we will discuss the effects of quantum interference and electron-electron coupling on the first three cumulants, e.g. the current $C_1(t)$, the zero frequency power spectrum $C_2(t)$ and the skewness $C_3(t)$ for a finite binning time of $t = 10$. A com-

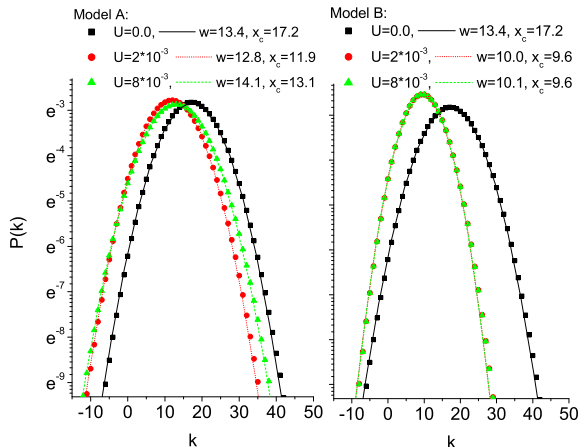


FIG. 4: Electron transfer probability $P^n(k, t)$ of the net-process for different electron-electron coupling strengths U as function of transferred electrons k . Left panel depicts Model A, right frame Model B. The time is set to $t = 200$. A small bias is applied $V = 4 \cdot 10^{-4}$. $w := \text{variance}$ and $x_c := \text{position of peak}$ are the fit parameters of the Gaussian. In Model B, the curves for $U = 2 \cdot 10^{-3}$ and $U = 8 \cdot 10^{-3}$ overlap.

parison of the results of Model A (Fig. 5) with Model B (Fig. 6) demonstrates the influence of interference. The skewness is of special interest since it was found to be the most sensitive of the three¹⁹. The upper panels of Figs. 5,6 depict the current through the left lead for three different processes: λ_+ counts the ingoing, λ_- the outgoing electrons, λ_n results in the statistics of the net-process. The voltage is $V = 1 \cdot 10^{-3}$. U introduces an energetic penalty for double occupancy. This explains the current drop in both models which occurs around $U = 2 \cdot 10^{-3}$ by the fact that the eigenenergy of the double occupancy state increases with U . This reduces the occupancy of the state and reduces its contribution to the total average current. The drop is smooth due to the finite temperature. Interesting effects can be observed at the intermediate regime. So is the drop of the net-current accompanied with an increase of the reverse current. The shot-noise follows qualitatively the current profile in Model A and B. In Model B, the skewness related to λ_n and λ_+ follows the current profile and decay until the strong Coulomb blockade is reached.

The first two cumulants deviate only slightly between Fig. 6 and Fig. 5. However, the skewness shows a qualitative different behavior at finite binning times. Following an initial drop, it oscillates back. This effect occurs only at finite binning times as one can see from a comparison with the asymptotic values of C_3 , shown in the bottom panel of Figs. 6,5. The asymptotic values were calculated from the eigenvalues of propagator (32) as described in section (IV).

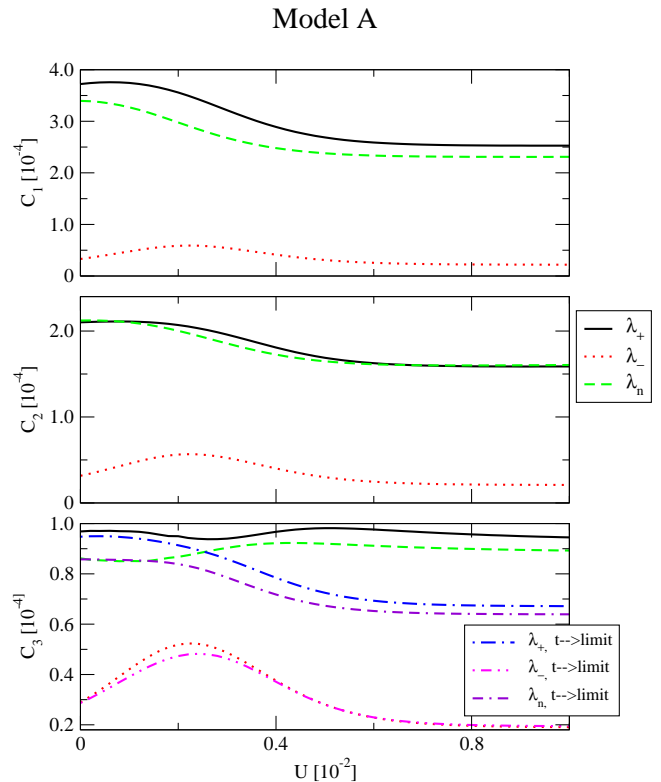


FIG. 5: First three cumulants, the current $C_1(t)$, the shot noise $C_2(t)$ and the skewness $C_3(t)$ as functions of electron-electron coupling U for a finite binning time of $t = 10$. The bottom panel also shows the asymptotic values (denoted by $t \rightarrow \infty$) of the skewness C_3 . λ_+ includes the incoming, λ_- the outgoing, and λ_n the net-process into the statistics of electron transfers between the system and the left lead. The bias voltage is $V = 1 \cdot 10^{-2}$.

C. Elementary probabilities

Using the expressions (40-42), we calculate the conditional elementary probabilities of directionally resolved consecutive electron transfers. Fig. 7 compares the elementary probabilities $P_{l \rightarrow r}(t, t_0)$, $P_{r \rightarrow l}(t, t_0)$, $P_{l \rightarrow l}(t, t_0)$ for the two models for a small bias of $V = 2 \cdot 10^{-3}$. In Model B, we observe an almost exponential decay of the probability of an outgoing electron transfer event at the left/right/left site following an incoming electron transfer event at t_0 at the right/left/left site. A small non-exponential slope indicates a weak correlation between the transfer processes. The probabilities of the reverse processes $r \rightarrow l$ decay faster than transfer in direction of the bias voltage $l \rightarrow r$. Consequently, the $l \rightarrow l$ process has an intermediate decay rate. Electron-electron coupling leads to a slower decay in all three processes, indicating that increasing U increases the probability of an electron to reside longer within the junction. The probability has its maximum at t_0 since the orbitals are in direct contact with both leads. For spatially extended wires, the maximum of the probability is delayed by the

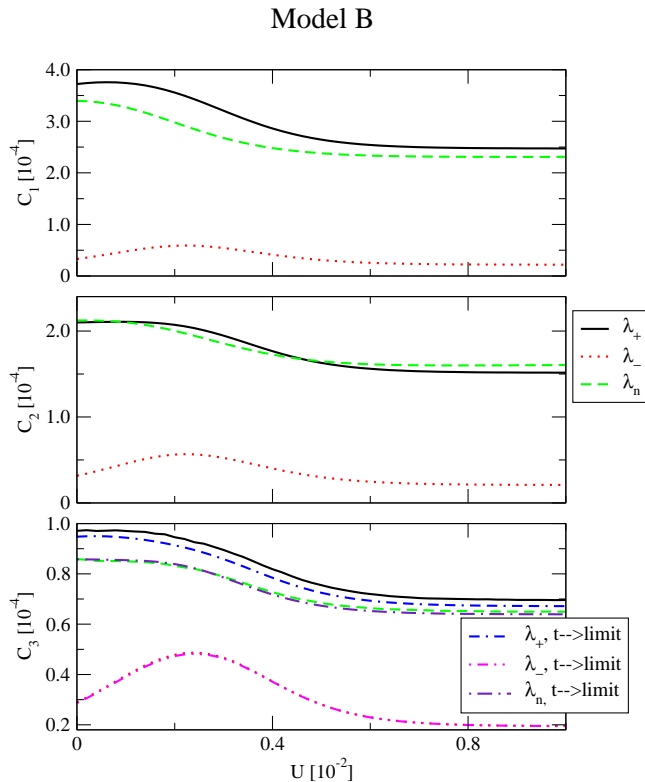


FIG. 6: Same quantities in as Fig. 5 but calculated for Model B.

average time required to propagate the electron through the system. In the Model A, the exponential decay of the probability is superimposed by an oscillation due to orbital interference. The amplitude of the oscillation is increased by Coulomb interaction.

Integrating the elementary probabilities depicted in Fig. 7 over time t gives the probability $P_{m_1 \rightarrow m_2}^c$ to find consecutive transfer events $m_1 \rightarrow m_2$ regardless of the time-interval between m_1 and m_2 . The upper panel of Fig. 8 depicts $P_{m_1 \rightarrow m_2}^c$ as a function of external bias voltage for Model A. The bottom panel shows the corresponding results for Model B. The two transfer processes under consideration are $l \rightarrow r$, $r \rightarrow l$, and we use $U = 0.0$ and $U = 2 \cdot 10^{-3}$ for comparison. Since the probability in Eq. (43) is conditional with respect to the first transfer, the $r \rightarrow l$ and $l \rightarrow l$ processes are equal. In the absence of an external voltage, all quantities are equal and are driven by the thermal fluctuations of the leads at finite temperature. A splitting occurs when the voltage is turned on. The deviations caused by the electron-electron coupling vanish in the high bias limit in both models.

Fig. 9 uses the same parameters as Fig. 8, but the observables are shown as functions of the electron-electron coupling U and the bias voltage is fixed at $V = 2 \cdot 10^{-3}$. The upper panel depicts the time-integrated two point probabilities, the bottom panel the average residence times for Model A and B. Increasing U causes a dip of

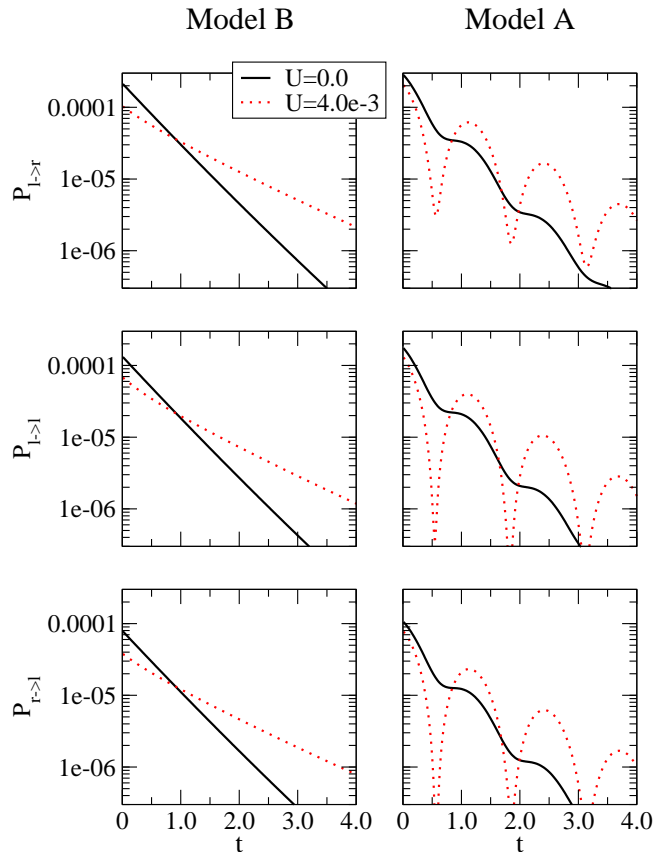


FIG. 7: Elementary probabilities $P_{l \rightarrow r}(t, t_0)/P_{l \rightarrow r}(t, t_0)$ for an electron entering the junction through the left/right/left lead at time t_0 leaving through the right/left/left at time t , respectively. The three panels on the left are calculated for Model B, the right side shows Model A. The bias voltage is $V = 2 \cdot 10^{-3}$.

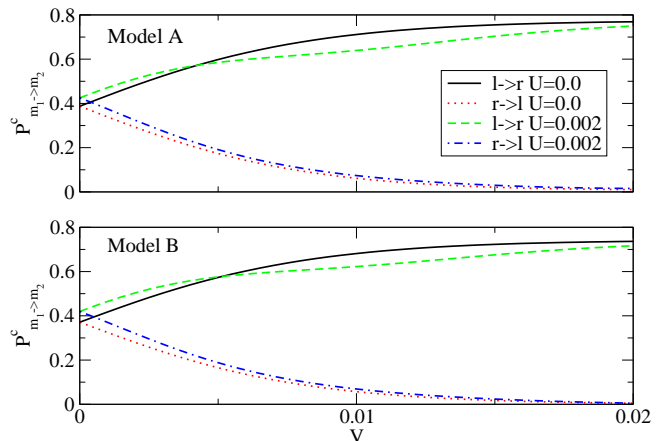


FIG. 8: Time-integrated two point probabilities (Eq.43) $P_{l \rightarrow r}^c$ and $P_{r \rightarrow l}^c$ as a function of bias voltage for different electron-electron coupling strength U . Upper panel Model A, bottom panel Model B.

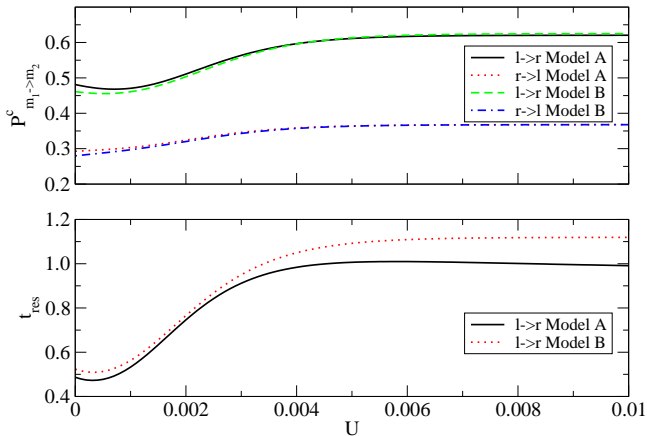


FIG. 9: Upper panel: Time-integrated two point probabilities (Eq.43), $P_{l \rightarrow r}$ and $P_{r \rightarrow l}$ versus electron-electron coupling strength U . Bottom panel: The mean residence time t_{res} of an electron in the system as a function of U for the different processes and Model A and B. The bias is $V = 1 \cdot 10^{-2}$

the $l \rightarrow r$ probabilities around $U = 2 \cdot 10^{-3}$. There are no qualitative differences between the probabilities of the two models. U strongly affects the mean residence time of the electrons which is also sensitive to the presents of orbital interferences. Thus the residence time between the electron entering and leaving the junction provides a useful measure for the electron-electron coupling. Also, it indicates the presence of quantum mechanical interferences in the transport of the system under investigation.

Fig. 10 depicts the conditional probability, Eq. (46), for an electron entering the junction through the left lead at time t_0 and next electron entering at time t . The detector is only applied to the left lead, transfers at the right lead are permitted at all times. Models A and B are compared for different U . The probabilities of Poissonian two-electron transfers, Eq. (47) are shown for comparison. Similar to the configuration with electron detectors at both leads, Fig. 7, one observes longer tails in the probability distribution in time for larger U . The transfer is strongly correlated at short times what leads to small probabilities for the next electron to enter the junction right after the first one has entered. At intermediate times, the probability is larger than the probability of the Poissonian process. For long times, the transfer becomes weakly correlated and the probabilities for Model A and B are close to a Poissonian distribution. Large oscillations can be observed due to orbital interference in Model A. The oscillations can be observed for longer times when Coulomb coupling is present. Using a time-sensitive detector and measuring a long time series of sequential electron transfers through one lead, those oscillations might be recovered in experiments employing time-series analysis. Long tails indicate presence of Coulomb interaction in the system, oscillations presence of interferences.

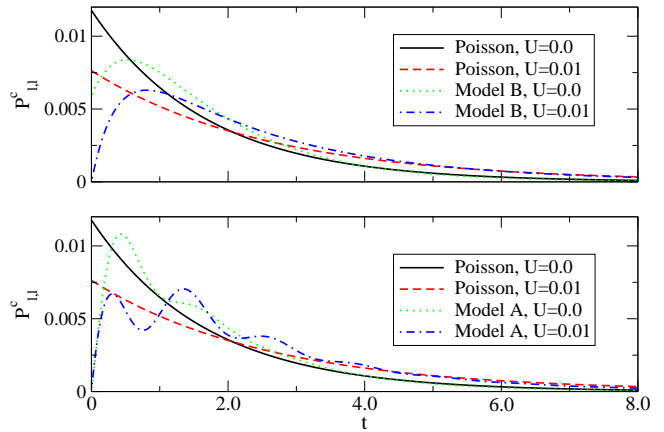


FIG. 10: Conditional probabilities $P_{l,l}^c(t|t_0)$ for an electron entering the junction through the left lead at time t_0 and the next electron enters at t . The electron detector keeps only track of transfers through the left lead. Electrons are allowed to leave and enter through the right lead at all times. Model A and B are compared for different U . For comparison, we also plot the corresponding Poissonian processes $P_{l,l}^{Poisson}(t|t_0)$. The bias voltage is $V = 2 \cdot 10^{-3}$.

D. The fluctuation theorem

Fig. 11 shows $K(t, \lambda_n)$, given in Eq. (34), for the net process as a function of λ for different electron-electron coupling strengths. Note that we rescale the x-axis by the fixed bias $V = 2 \cdot 10^{-3}$. To explore the role of interferences we compare Models A and B. $K(t, \lambda_n)$ for the finite time $t = 10$ was calculated by propagation the EOM (31) of the GO, the limit $\lim_{t \rightarrow \infty} K(t, \lambda_n)$ is computed from the eigenvalues of $W(\lambda_n)$. We observe that finite electron-electron coupling, $U = 2 \cdot 10^{-3}$, significantly changes $K(t, \lambda_n)$ and the influence of Coulomb blockade can be measured in the first cumulant of GF, the current. The effects due to the interference terms are smaller and only occur at finite times if $U \neq 0$. In this regime, a discrepancy between Model A and B can be observed for larger λ which indicates that it is significant in higher cumulants, here the third as shown in Fig. (5). We find that at infinite time the symmetry $K(t, \lambda) = K(t, \lambda - \beta V)$ holds in both models. This confirms that the fluctuation theorem, $\frac{P(k)}{P(-k)} = \exp(\beta V k)$, for $t \rightarrow \infty$, is satisfied even in the presence of electron-electron coupling and interferences.

VII. CONCLUSIONS

We have calculated the counting statistics for arbitrary electron-electron coupling strength, bias voltages and finite temperatures. Including the coherence elements in the GF, the numerical results reveal the importance of the quantum interference terms on the statistics. These effects could be measured using the proposed arrange-

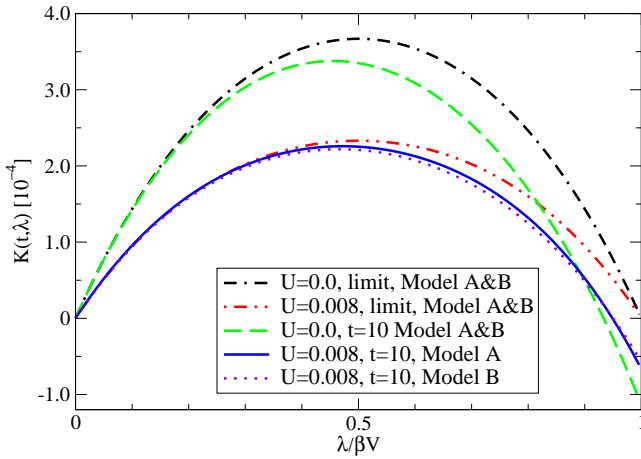


FIG. 11: $K(t, \lambda_n)$ calculated for different values of t and electron-electron interaction U as a function of λ . The results for finite time $t = 10$ are obtained by propagation of $K(t, \lambda_{1-2})$, the limit $\lim_{t \rightarrow \infty} K(t, \lambda_n)$ is given by the eigenvalue E_{λ_n} of $G(t, \lambda_n)$, with $E_{\lambda_n} \rightarrow 0$ for $\lambda_n \rightarrow 0$. The x-axis is rescaled by βV .

ment of two or more QDs. In particular the skewness shows qualitative different behavior. We also show that a measurement of the average residence time of electrons is affected by quantum mechanical interference as well as the Coulomb coupling between two parallel quantum dots. Detecting a large number of electron transfers, oscillations in the elementary transfer probabilities caused by orbital interference might be recovered by time-series analysis. Our simulations indicate that the reverse-transfer can be increased by the Coulomb coupling if the energy settings of the system are tuned correctly.

Several possible extensions of the model are of interest. Decoherence effects can be included by coupling a dissipative phonon bath to the sites. Including higher order coupling elements beyond second-order perturbation theory in the GF could reveal more insights in the dynamics of the system-lead contact.

Acknowledgments

The support of the National Science Foundation (Grant No. CHE-0446555, CBC-0533162) and NIRT (Grant No. EEC 0303389) is gratefully acknowledged. M.E. was partially supported by the FNRS Belgium (collaborateur scientifique)

APPENDIX A: NUMERICAL DECOMPOSITION

In Model B, the trace over the lead degrees of freedom and all the reservoir operators in the dissipation term of Eq. (10) can be recast in terms of correlation functions of

the form

$$C_{\sigma\sigma'}^{(+)}(t) = \sum_q V_{q\sigma} V_{q\sigma'}^* \langle \Psi_{q\sigma'} e^{-iH_R t} \Psi_{q\sigma}^\dagger e^{iH_R t} \rho_R \rangle_R \quad (\text{A1})$$

$$C_{\sigma\sigma'}^{(-)}(t) = \sum_q V_{q\sigma} V_{q\sigma'}^* \langle e^{-iH_R t} \Psi_{q\sigma}^\dagger e^{iH_R t} \Psi_{q\sigma'} \rho_R \rangle_R \quad (\text{A2})$$

The properties of the trace lead to $C_{\uparrow\downarrow}^{(\pm)} = C_{\downarrow\uparrow}^{(\pm)} = 0$. While not an approximation, the procedure mimics a rotating wave approximation in Eq. (23). The reservoir correlation functions in Model A used in Eqs. (12,13) are given by

$$C_{ss'}^{(+)}(t) = \sum_q T_{qs} T_{qs'}^* \langle \Psi_q e^{-iH_R t} \Psi_q^\dagger e^{iH_R t} \rho_R \rangle_R \quad (\text{A3})$$

$$C_{ss'}^{(-)}(t) = \sum_q T_{qs} T_{qs'}^* \langle e^{-iH_R t} \Psi_q^\dagger e^{iH_R t} \Psi_q \rho_R \rangle_R \quad (\text{A4})$$

The coupling to the two dots is assumed to be symmetric $T_{q1} = T_{q2}$. Contrary to Eqs. (A1,A2), the correlation functions for the cross coupling terms are unequal zero: $C_{ss'}^{(\pm)}(t-t') = C_{ss}^{(\pm)}(t-t')$. The following derivations refer to Eqs. (A1,A2). The same procedures have to be applied to Eqs. (A3,A4) as well but we will not present them in detail. All the external properties of the fermionic reservoir are described by a single quantity, namely the spectral density $J_R(\omega)$, which can be generated by a superposition of weighted δ -functions

$$J_R(\omega) = \sum_q \pi |V_q|^2 \delta(\omega - \omega_q). \quad (\text{A5})$$

We apply a numerical decomposition of the spectral density to derive equations of motion

$$J_R(\omega) = \sum_{k=1}^m p_k \frac{\Gamma_k^2}{(\omega - \Omega_k)^2 + \Gamma_k^2}. \quad (\text{A6})$$

With the complex roots of the Fermi function and of function (A6), the theorem of residues applied to Eqs. (A1, A2) results in³⁴

$$C_{\sigma\sigma'}^{(+)}(t) = \sum_{k=1}^m p_k \Gamma_k \left(n_F(-\Omega_k^- + E_F) e^{-i\Omega_k^- t} \right) - \frac{2i}{\beta} \sum_k^{m'} J_R(\nu_k^*) e^{-i\nu_k^* t} \quad (\text{A7})$$

$$C_{\sigma\sigma'}^{(-)}(t) = \sum_{k=1}^m p_k \Gamma_k \left(n_F(\Omega_k^+ - E_F) e^{i\Omega_k^+ t} \right) - \frac{2i}{\beta} \sum_k^{m'} J_R(\nu_k) e^{i\nu_k t} \quad (\text{A8})$$

with the abbreviations $\Omega_k^+ = \Omega_k + i\Gamma_k$ and $\Omega_k^- = \Omega_k - i\Gamma_k$ and the Matsubara frequencies ν_k given by $\nu_k = i\frac{2\pi k + \pi}{\beta} + E_F$. In general, one has to take an infinite number of Matsubara frequencies into account, but it was demonstrated that the summation can be truncated³²⁻³⁴. From Eqs.(A7,A8), we can write the correlation functions as

$$C_{\sigma\sigma}^{(\pm)}(t) = \sum_{k=1}^{m+m'} a_k^{(\pm)} e^{\gamma_k^{(\pm)} t} \quad (\text{A9})$$

The same decomposition can be derived for $C_{ss'}^{(\pm)}(t)$:

$$C_{ss'}^{(\pm)}(t) = \sum_{k=1}^{m+m'} a_k^{(\pm)} e^{\gamma_k^{(\pm)} t}. \quad (\text{A10})$$

- ¹ J. Bylander, T. Duty, and P. Delsing, *Nature* **434**, 361 (2005).
- ² Z. J. W. Lu, L. Pfeifer, K. W. West, and A. J. Rimberg, *Nature* **423**, 422 (2003).
- ³ T. Fujisawa, T. Hayashi, Y. Hirayama, and H. D. Cheong, *Appl. Phys. Lett.* **84**, 2343 (2004).
- ⁴ S. Gustavsson, R. Leturcq, B. Simovic, R. Schleser, T. Ihn, P. Studerus, K. Ensslin, D. C. Driscoll, and A. C. Gossard, *Phys. Rev. Lett.* **96**, 076605 (2006).
- ⁵ T. Fujisawa, T. Hayashi, R. Tomita, and Y. Hirayama, *Phys. Rev. Lett.* **312**, 1634 (2006).
- ⁶ M. Esposito, U. Harbola, and S. Mukamel, *Phys. Rev. B* **75**, 155316 (2007).
- ⁷ L. S. Levitov and M. Reznikov, *Phys. Rev. B* **70**, 115305 (2004).
- ⁸ Y. M. Blanter and M. Buttiker, *Phys. Rep* **336**, 1 (2000).
- ⁹ S. A. Gurvitz, *Phys. Rev. B* **56**, 15215 (1997).
- ¹⁰ J. Wabnig, D. V. Khomitsky, J. Rammer, and A. L. Shelankov, *Phys. Rev. B* **72**, 165347 (2005).
- ¹¹ J. Rammer, A. L. Shelankov, and J. Wabnig, *Phys. Rev. B* **70**, 115327 (2004).
- ¹² A. L. Shelankov and J. Rammer, *Europhys. Lett.* **63**, 485 (2003).
- ¹³ C. Flindt, T. Novotny, and A.-P. Jauho, *Europhys. Lett.* **69**, 475 (2005).
- ¹⁴ G. Kiesslich, P. Samuelsson, A. Wacker, and E. Schoell, *Phys. Rev. B* **73**, 033312 (2006).
- ¹⁵ Y. Utsumi, D. S. Golubev, and G. Schoen, *Phys. Rev. Lett.* **96**, 086803 (2006).
- ¹⁶ J. N. Pedersen and A. Wacker, *Phys. Rev. B* **72**, 195330 (2005).
- ¹⁷ C. Groth, B. Michaelis, and C. Beenakker, "counting statistics of coherent population trapping in quantum dots", *cond-mat/0605630*.
- ¹⁸ D. Bagrets and Y. Nazarov, *Phys. Rev. B* **67**, 085316 (2003).
- ¹⁹ S. Wang, H. Jiao, F. Li, X. Li, and Y. Yan, *Full counting statistics of transport through two-channel coulomb blockade systems*, *cond-mat/0703745*.
- ²⁰ M. Esposito and S. Mukamel, *Phys. Rev. E* **73**, 046129 (2006).
- ²¹ C. Jarzynski, *Phys. Rev. Lett.* **78**, 2690 (1997).
- ²² G. Gallavotti and E. G. D. Cohen, *Phys. Rev. Lett.* **74**, 2694 (1995).
- ²³ J. L. Lebowitz and H. Spohn, *J. Stat. Phys.* **95**, 333 (1999).
- ²⁴ D. J. Searles and D. J. Evans, *Phys. Rev. E* **60**, 159 (1999).
- ²⁵ U. Seifert, *Phys. Rev. Lett.* **95**, 040602 (2005).
- ²⁶ U. Harbola, M. Esposito, and S. Mukamel, *Phys. Rev. B* **74**, 235309 (2006).
- ²⁷ J. Jin, S. Welack, J. Luo, X. Li, P. Cui, R. Xu, and Y. Yan, *J. Chem. Phys.* **126**, 134113 (2007).
- ²⁸ C. Bruder and H. Schoeller, *Phys. Rev. Lett.* **72**, 1076 (1993).
- ²⁹ J. Lehmann, S. Kohler, P. Hänggi, and A. Nitzan, *Phys. Rev. Lett.* **88**, 228305 (2002).
- ³⁰ X.-Q. Li, J.-Y. Luo, Y.-G. Yang, P. Cui, and Y. Yan, *Phys. Rev. B* **71**, 205304 (2005).
- ³¹ P. Cui, X. Q. Li, J. Shao, and Y. Yan, *Phys. Lett. A* **357**, 449 (2006).
- ³² C. Meier and D. J. Tannor, *J. Chem. Phys.* **111**, 3365 (1999).
- ³³ U. Kleinekathöfer, *J. Chem. Phys.* **121**, 2505 (2004).
- ³⁴ S. Welack, M. Schreiber, and U. Kleinekathöfer, *J. Chem. Phys.* **124**, 044712 (2006).
- ³⁵ X. Li and Y. Yan, *Phys. Rev. B* **75**, 075114 (2007).
- ³⁶ U. Kleinekathöfer, G.-Q. Li, S. Welack, and M. Schreiber, *phys. stat. sol.* **243**, 3775 (2006).
- ³⁷ S. Mukamel, *Phys. Rev. Lett.* **90**, 170604 (2003).
- ³⁸ G. Gardiner and P. Zoller, *Quantum Noise* (Springer, 2004).
- ³⁹ I. Bronstein, K. Semendjajew, G. Musiol, and H. Muehlig, *Taschenbuch der Mathematik* (Verlag Harry Deutsch, 2001).